Neural Comput & Applic (2007) 16:541–549
DOI 10.1007/s00521-007-0103-0

ICONIP2006

Modeling hemodynamic variability with fuzzy features for detecting brain activation from fMR time-series

Juan Zhou · Jagath C. Rajapakse

Received: 20 November 2006 / Accepted: 2 March 2007 / Published online: 8 September 2007

Abstract We propose to detect brain activation from fMR time-series of a group study by modeling fuzzy features. Five discriminating features are automatically extracted from fMRI data by a sequence of temporal-sliding-windows. A fuzzy model based on these features is first derived by a gradient method on a set of initial training data and then incrementally enhanced. The resulting fuzzy activation maps of all subjects are then combined to provide a measure of strength of activation of each voxel, based on the group of subjects. A two-way thresholding scheme is introduced to determine true activated voxels. The method is tested on both synthetic and real fMRI datasets. The method is less vulnerable to correlated noise and able to capture the key activation from a group of subjects by adapting to hemodynamic variability across subjects.

1 Introduction

Functional magnetic resonance imaging (fMRI) is a non-invasive technique measuring functional activity of the brain in vivo, both spatially and temporally. The signal is based on the blood-oxygenation-level-dependent (BOLD) contrast, derived from the increase in blood oxygenation followed by neuronal activity, resulting in a change of magnetic resonance (MR) signal. The detection of fMRI signal is not trivial as BOLD signal change due to a typical experimental stimulation of the brain is very subtle, ranging from 1 to 5% on a 1.5 T scanner [14]. Furthermore, various noise and artifacts such as motion, electronic, physical, and physiological processes significantly confound the fMRI signal. Therefore, techniques for fMRI analysis should be insensitive to the uncertainties and fuzziness introduced by these interference signals.

Two groups of methods have been used to detect activated voxels in fMRI data: hypothesis-driven and data-driven. Statistical parametric mapping (SPM) is the most widely used hypothesis-driven method for fMRI analysis, which assumes a linear regression model for the fMR signal with a specific noise structure. It is voxel-based and tests the hypothesis about fMR time-series by construction and assessment of spatially extended statistical processes based on Gaussian random fields (GRF) [6]. Markov random fields (MRF) [19] and Conditional random fields (CRF) [24] have been attempted to account for contextual dependencies among activated voxels or data, respectively. However, it has become clear that there is a nonlinear relationship between the variation in the fMRI signal and the stimulus presentation [21]; and the hemodynamic response function (HRF) varies spatially and between subjects [22]. Moreover, the structure of noise in fMRI is not well understood and remains a contentious subject [3]. Thus, the validity of the statistical models depends on the extent to which the data satisfies the underlying assumptions.

In contrast, data-driven methods do not assume any prior knowledge of hemodynamic behaviors and are considered more powerful and relevant for fMRI studies in which

J. Zhou · J. C. Rajapakse (✉)
BioInformatics Research Centre,
Nanyang Tecnological University,
Singapore, Singapore
e-mail: asjagath@ntu.edu.sg

J. C. Rajapakse
Singapore-MIT Alliance, Singapore, Singapore

unknown or complex differential responses are expected [12]. Generally, these data-driven methods can be divided into two groups: transformation-based and clustering-based. Principle component analysis (PCA) [1] and independent component analysis (ICA) [8, 9, 11] belongs to the first group, which transform the original high-dimensional input space in order to separate functional responses and various noise sources from each other. ICA is an information theoretic approach which enables recovery of underlying signals or independent components from linear data mixtures. It has been applied to fMRI analysis both spatially [11] and temporally [4], as well as with constraints [8]. The second clustering group consists of fuzzy clustering [5] and self-organizing map [13], attempting to classify time signals of the brain into several patterns according to temporal similarity. For these data-driven methods, usually the contents of one class or component are interpreted as activations but how the signal is divided into classes is difficult to ascertain or comprehend. Certain class with a particular activation pattern has physiological interpretation but others are still unknown. Other fMRI analysis methods include specified-resolution wavelet analysis [7] and Bayesian modelling [22].

The motivation behind the present work is to develop a technique for brain activation detection from fMRI data that is less vulnerable to noise and hemodynamic variability than hypothesis-driven methods and more interpretable than previous data-driven methods. Because of the complex, nonlinear, and imprecise nature of signal and noise, modeling fMRI signal accurately by a conventional nonlinear mathematical approach is a difficult task, especially in this case with limited prior knowledge. In contrast, fuzzy modeling is a plausible way to model uncertainty of fMRI data using limited available information. Moreover, methods based on raw fMRI data are often computational complex and vulnerable to noise. The proposed feature extraction from time-series is able to lower the computational complexity and enhance system ability in handling noise. In order to account for HRF variability across subjects, incremental learning is used so that the fuzzy model could adapt to individual subject in order to better identify common activated regions. Here, we propose a novel approach of fuzzy feature modelling (FFM) to detect activated voxels in human brain, which consists of (1) extracting features based on temporal-sliding-windows (TSW) from fMR time-series; (2) fuzzy feature modeling by incremental learning; and (3) thresholding on fuzzy activation map. In addition, we have extended our previous work [26] to group study of fMR time-series where fusion of fuzzy activation maps of the subjects is performed before thresholding. The details of our approach is described in next section. In Sect. 7 the performance of this approach is illustrated with functional activation detection for individual and group study on both synthetic and real fMRI data.

2 Method

2.1 Extracting features

Different voxels have different hemodynamic characteristics, for example, the signal magnitude at activated or non-activated states and hemodynamic response time to reach its peak could differ. The principle behind our feature extraction is a sequence of TSW shifting over a time-series, from which consistent discriminating features for the activated and non-activated voxels of each condition could be derived regardless of different shape, magnitude, or delay of hemodynamic response function. Let $\Psi : \Omega \times \Theta \rightarrow Y$ be a functional time-series where $\Omega \subset N^3$ denotes the three-dimensional spatial domain of image voxels, $\Theta = \{1, 2, \ldots, n\}$ indexes n number of 3D scans taken during the experiment. Let $Y = \{y_{i,t} : i \in \Omega, t \in \Theta, y_{i,t} \in Q\}$ be a 4D data where Q denotes the range of image intensities and $y_{i,t}$ represents the intensity of voxel i at time t. Let Ω_B denote the set of brain voxels.

Here, we consider an experiment with one condition denoted by X for notational simplicity; the algorithm is also applicable for fMR time-series with a number of conditions [26]. The condition X is presented together with resting state alternatively or randomly for P times in a single run while n 3D brain scans are taken, so each block of condition X is denoted by B_p, p = 1,2,...,P. Block B_p lasts for a duration of length l_p and the beginning of block B_p is denoted as b_p where p = 1,2,...,P. The above represents a general paradigm design which applies to both block and event-related designs. Then, a sequence of TSW for the condition X is constructed from fMR time-series as follows:

1. Create a sequence of P number of windows denoted by $W = \{W_p : p = 1,2,...,P\}$; in other words, one window W_p for each condition block B_p. The length of window W_p is denoted by w_p and $w_p = l_p$, i.e., equals to the duration l_p of each block B_p. The initial starting point of window W_p is thus given by b_p.
2. Shift the sequence of windows W temporally forward by a sliding time interval s simultaneously, resulting in a new sequence of windows denoted by $W(s) = \{W_p(s): s = 0,1,...,S,\ p = 1,2,...,P\}$. Depending on different inter-scan time, the maximum sliding time interval S varies: $S = 32/RT$ (seconds) based on the fact that the total length of hemodynamic response function is approximately 32 s. Thus, the starting and ending time

of window $W_p(s)$ is $b_p + s$ and $b_p + s + w_p$–1, denoted by $T_{p,1}(s)$ and $T_{p,2}(s)$ respectively for simplicity reason.

3. For each window $W_p(s)$ as $s = 0,1,...,S$, calculate the average intensity $A_p(i,s)$ of each voxel i as:

$$A_p(i,s) = \frac{\sum_{t=T_{p,1}(s)}^{\tilde{T}_{p,2}(s)} y_{i,t}}{\tilde{T}_{p,2}(s) - T_{p,1}(s)} \tag{1}$$

where $\tilde{T}_{p,2}(s) = \min\{n, T_{p,2}(s)\}$.

Thus, we can observe a curve $A_p(i) = \{A_p(i,s): s = 0,1,...,S\}$ for each voxel i in each condition block B_p, whose shape is highly discriminating between activated and non-activated voxels. We call it Quasi-hemodynamic curve (QHC) since it is similar to HRF in general sense. Five discriminating features $F_k^p(i)$, $k = 1,2,...,5$, are extracted from this QHC for each voxel i in each condition block B_p as follows:

1. Area under curve ratio for QHC:

$$F_1^p(i) = \frac{\sum_{s=0}^{\tilde{w}_p} A_p(i,s)}{(\max_s A_p(i,s) - \min_s A_p(i,s)) \cdot \tilde{w}_p} \tag{2}$$

where $\tilde{w}_p = \min\{w_p, S\}$.

2. Area difference ratio for QHC:

$$F_2^p(i) = \frac{\sum_{s=0}^{\tilde{w}_p} A_p(i,s)}{\sum_{s=\tilde{w}_p+1}^{S} A_p(i,s)} \tag{3}$$

3. Correlation between QHC $A_p(i)$ and the standard QHC, SA_p:

$$F_3^p(i) = \frac{\sum_{s=0}^{\tilde{w}_p}(A_p(i,s) - \overline{A_p(i,s)})(SA_p - \overline{SA_p})}{\sqrt{\sum_{s=0}^{\tilde{w}_p}(A_p(i,s) - \overline{A_p(i,s)})^2 \sum_{s=0}^{\tilde{w}_p}(SA_p - \overline{SA_p})^2}} \tag{4}$$

where $SA_p = \{SA_p(s) = -(s - \tilde{w}_p/2)^2 : s = 0, 1, \ldots, \tilde{w}_p\}$.

4. Time ratio at peak amplitudes of QHC:

$$F_4^p(i) = \arg_{s \in [0,\tilde{w}_p]} \max_s A_p(i,s)/\tilde{w}_p \tag{5}$$

5. Time ratio at lowest amplitude for QHC:

$$F_5^p(i) = \arg_{s \in [0,\tilde{w}_p]} \min_s A_p(i,s)/\tilde{w}_p \tag{6}$$

Two curves have been normalized to [0,1] before correlation computation in feature 3 for easy comparison among voxels. Since the shapes of QHC of an activated and non-activated voxel are usually different as seen later, the above five features could be significantly discriminating.

The above five features of each block are sum up over all blocks as in Eq. 7, leading to a robust 5D feature space as fuzzy features are less vulnerable to noise or changes in HRFs. Note that we assume the duration of each block $l_p \leq S$ in the above definitions. For cases like $l_p > S$, we should apply the opposite settings, i.e., use window length $w_p = 32$/RT and the maximum sliding time for each window $S_p = l_p$. The properties of the resulting curve is similar to QHC and same features could be extracted.

$$F_k(i) = \sum_{p=1}^{P} F_k^p(i)/P \tag{7}$$

2.2 Learning fuzzy activation maps

Based on the feature space developed in the previous section, we use a gradient technique to derive a fuzzy feature model. A new incremental learning scheme is proposed to extract useful knowledge not only from a set of standard HRFs with various parameters but also from fMRI data of each subject itself. This scheme is able to adapt to the hemodynamic variability across subjects by building one fuzzy model for each subject. The resulting fuzzy model is able to (1) calculate the strength of activation of each voxel to each condition and (2) provide a rule-base for interpretation of activation patterns. For each condition X, one five-input $F(i) = \{F_k(i) : k = 1,2,...,5\}$, single-output $Z(i)$ (activation strength), fuzzy model M is developed for all voxels $i \in \Omega_B$. The proposed incremental learning scheme to derive model M is as follows:

1. *Building initial training data*: For the class of activated voxels, randomly select parameters of the canonical HRF within a certain range to create a set of time-series, consisting of H different variations of original HRF, e.g., time and dispersion derivatives. Add all these time-series to the initial training set with the desired output D as 1. For initial training time-series of the class of non-activated voxels, time-series of constant amplitude in the range [0,1] are added to the initial training set with the desired output D as 0. The initial test set is the time-series of all brain voxels in the target subject, denoted by $Y = \{y_{i,t} : i \in \Omega_B, t \in \Theta\}$.
2. *Extracting features*: For incremental learning iteration r, extract features from training data as described in Sect. 2.1.
3. *Training*: Apply gradient method (GM) to train the fuzzy model M based on the extracted features until the convergence criterion are met. The objective of GM based training is to minimize the error between the predicted output value $Z(i)$ and the desired output value $D(i)$ for each voxel i in the training set:

$$\epsilon = \frac{1}{2}\left[Z(i) - D(i)\right]^2 \tag{8}$$

Gaussian fuzzy membership functions are presumed for input features as in Eq. 9 and the mechanism of fuzzy

model M employs a product t-norm for the input features (premise of the rule base) and a product implication as in Eq. 10. Delta output fuzzy membership function is used.

$$\mu_k(i) = \exp\left[-\frac{1}{2}\left(\frac{F_k(i) - \alpha_k}{\sigma_k}\right)^2\right] \tag{9}$$

$$Z(i) = \frac{\sum_{c=1}^{2} \beta_c \prod_{k=1}^{5} \mu_k(i)}{\sum_{c=1}^{2} \prod_{k=1}^{5} \mu_k(i)} \tag{10}$$

where $c = 1$ and $c = 2$ denotes the classes of activated and non-activated voxels for the condition of interests, respectively. Therefore, parameters of the fuzzy model include input center α_k, input variance σ_k and output center β_c, where $c \in \{1,2\}$ and $k = 1,2,...,5$. GM is able to tune these parameters of the fuzzy model and detailed parameter updating equations can be found in [15].

4. *Testing*: Feed the extracted features from testing data at current round to the resulting fuzzy model M in step 3 to determine output.
5. *Updating training data*: Select the top m activated voxels and non-activated voxels in terms of high or low outputs and add into the training set of next round. The desired output is again 1 for activated voxels and 0 for non-activated voxels, respectively. Meanwhile, remove these points from the testing set. Repeat steps 2–5 till certain criteria is reached, e.g., maximum incremental learning round is reached or no more suitable voxels can be added into training set.
6. *Final testing*: Apply the whole fMRI data to the final fuzzy model once more to obtain finalized output $Z = \{Z(i) : i \in \Omega_B\}$.

2.3 Detecting activation

In order to detect activation by thresholding, a half-triangular fuzzy membership function is designed to convert original activation strength map $Z(i)$ to a fuzzy activation map $Z^* = \{Z^*(i): i \in \Omega_B, Z^*(i) \in [0,1]\}$ as in Eq. 8 where 1 for activated voxels and 0 for non-activated voxels. This map represents the activation strength of each voxel in terms of fuzzy membership values, which enables a rather consistent and effective performance across different data by the following two-way thresholding method.

First, a simple thresholding is applied as in Eq. 12 based on two parameters ζ_1 and ζ_2 ($\zeta_1 > \zeta_2$) for adding high confident voxels to the set of activated voxels Υ_1 and the set of non-activated voxels Υ_2. Then, for undetermined voxels i where $Z^*(i) < \zeta_1$ & $Z^*(i) > \zeta_2$, an ordered list is formulated based on the value of $Z^*(i)$. A screen process begins simultaneously from the two ends of this list and assign voxels in the list to be activated or non-activated according to Eq. 13.

$$Z^*(i) = \begin{cases} 1 & \text{if } Z(i) >= b_1 \\ (Z(i) - b_2)/(b_1 - b_2) & \text{if } Z(i) < b_1 \text{ and } Z(i) > b_2 \\ 0 & \text{if } Z(i) <= b_2 \end{cases} \tag{11}$$

$$\beta(i) = \begin{cases} 1 & \text{if } Z^*(i) >= \zeta_1 \\ 0 & \text{if } Z^*(i) <= \zeta_2 \end{cases} \tag{12}$$

$$\beta(i) = \begin{cases} 1 & \text{if } \chi(1,i,v) > \chi(0,i,v) \\ 0 & \text{if } \chi(1,i,v) < \chi(0,i,v) \end{cases} \tag{13}$$

where $c = \{0,1\}; \chi(c,i,v) = \prod_{j \in \varphi(i,v), j \in \Upsilon_c, \beta(j)=c} |Z^*(j) - Z^*(i)| \cdot \text{distance}\,(i,j)$; $\varphi(i,v)$ is the neighborhood of voxel i within a cube of size v^3. Each voxel i is removed from list and added into the set of activated voxels Υ_1 or the set of non-activated voxels Υ_2 accordingly and the screen continues until there is no more voxels in the list.

2.4 Group study

In order to detect common activated brain regions from a group of subjects, the fusion of the fuzzy activation maps Z^* of each subject is required to form a combined fuzzy activation map $Z^*_{\text{group}} = \{Z^*_{\text{group}}(i): i \in \Omega_B, Z^*_{\text{group}}(i) \in [0,1]\}$ as:

$$Z^*_{\text{group}}(i) = \left(\prod_{j=1}^{J} Z^*_j(i)\right)^{1/J} \tag{14}$$

where J equals the number of subjects in the group. Note that the activation map is normalized to [0,1] after fusion and the same thresholding procedure in Sect. 2.3 can be applied to this combined fuzzy activation map to identify brain activation.

3 Experiments and results

All simulations were done in MATLAB. Both synthetic and real fMRI data were used in experiments and a comparison between the results produced by our approach and statistical parametric mapping (SPM2) is given.

3.1 Synthetic data

A 2D synthetic functional dataset consisting six cycles (8 ON and 8 OFF, TR = 2 s, $n = 96$) was simulated. The response of the activated voxels was generated by convolving a box-car time-series with HRF, a mixture of two gamma functions, while the non-activated voxels kept

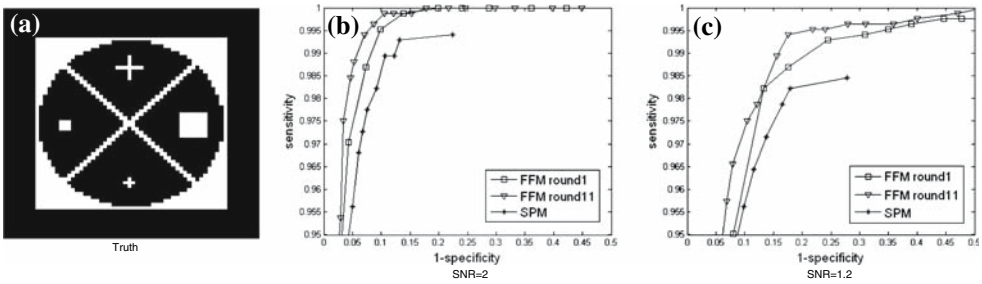

Fig. 1 ROC curve for detecting activation on synthetic functional data. *Triangular* and *square* curves represent results for round1 and round 11 of our FFM approach on original data, respectively; *asterisk* curve indicates results by SPM

unchanged at zero amplitude. True activation pattern generated is shown in Fig. 1a. Since the noise in fMRI time-series is often correlated, synthetic image with different levels of spatially correlated noise (by averaging the neighboring i.i.d. Gaussian noise) were tested. Five synthetic time-series were simulated based on different HRF by varying its parameters: the delay of response and undershoot relative to onset, the dispersion of response and undershoot, ratio of response to undershoot, and the total length of HRF function. The purpose is to test the vulnerability of fuzzy feature modeling (FFM) and SPM to the HRF variability across subjects.

The SPM analysis used the standard procedure implemented in SPM2 [20]. A 6 mm 3D Gaussian filter was applied to increase signal to noise ratio before statistical analysis. Canonical hemodynamic response with time and dispersion derivatives was used as basis function for statistical modeling. Confounding effects of fluctuations in global mean were removed by proportional scaling, and low frequency noise was removed with a high pass filter (128 Hz) applied to the fMRI time-series at each voxel. Specific effects were tested by applying appropriate linear contrasts, and *t*-statistical parametric maps were used to assess significant hemodynamic changes. We report activations in voxels below a threshold of $p < 0.05$, which were corrected for multiple comparisons using false discovery rate (FDR) [2].

To test the present FFM approach, 40 time-series (20 for activated class and 20 for non-activated class, i.e., $H = 20$) were used as initial training data set and $m = 10$ voxels were selected from each class and added into training set at each incremental learning round. This small value of m recruits fewer confounding voxels for training purpose. It is observed that as the incremental training in FFM approach proceeds, the fuzzy model can adapt to the data to a large extent at the expense of computational complexity but overfitting and performance deterioration could occur when confounding voxels are added to the training set. Thus, we use ten iterations of incremental learning. For step 3 in Sect. 2.2, initial conditions for fuzzy membership parameters are set to same values: input center $\alpha_k = F_k$ of the first training sample; input variance $\sigma_k = 1$; output center $\beta_1 = 1$ for the class of activated voxels and $\beta_2 = 0$ for the class of non-activated voxels. Parameters controlling the updating steps for α, σ and β were all initialized to 1. The GM training stops when the average error is less than 10^{-3} or the absolute changes between consecutive rounds is less than 10^{-5}. In Sect. 2.3, the neighborhood size for undetermined voxels is $v = 5$ and if no neighbors with known class is found, searching continues after increasing v by 1. However, the neighborhood was limited to 1/125 of whole brain volume.

The performance of FFM on a single subject is compared to SPM by plotting the ROC curves for functional activation detection. Figure 1b and c shows the results by thresholding on SPMs using different significance levels and on the final fuzzy activation map Z^* using various ζ_1 and ζ_2 for both correlated noise level SNR = 2.0 and 1.2. As seen, the present FFM approach outperforms SPM

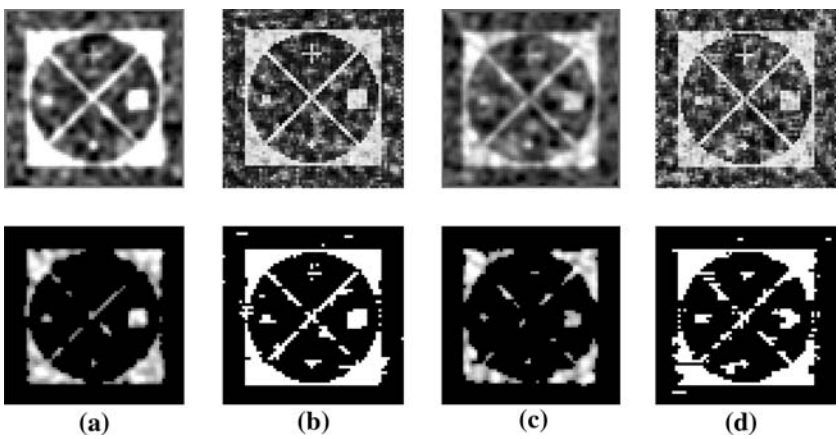

Fig. 2 Detected activation for synthetic data having correlated noise by **a** SPM at SNR = 2.0, **b** FFM at SNR = 2.0, **c** SPM at SNR = 1.2, and **d** FFM at SNR = 1.2. Row 1 are unthresholded SPMs and fuzzy activation maps while row 2 are thresholded activation maps for each case

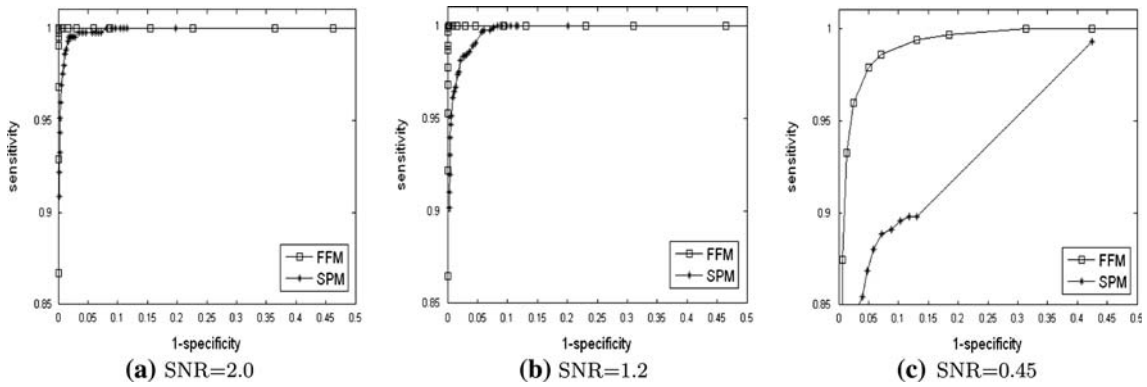

Fig. 3 ROC curve for detecting activation on a group study of five synthetic time-series with different HRFs. *Square* curve represents results by FFM and *asterisk* curve indicates results by SPM

for data at both noise levels; it is important to note that incremental training does improve the performance (comparing ROC of round 1 and round 11). Statistical parametric map and fuzzy activation map for this single subject are compared in row 1 of Fig. 2. The thresholded map produced by SPM (T-contrast with FDR $p < 0.05$) is compared to FFM ($\zeta_1 = 0.95$, $\zeta_2 = 0.3$) in row 2 of Fig. 2. It is observed that our approach is able to discover more important and detailed signal pattern than SPM, especially in high correlated noise case.

Statistical parametric mapping and FFM were also applied to detect activation from a group study of five synthetic time-series. Figure 3 illustrates ROC curves of both approaches on synthetic data with three levels of correlated noise: SNR = $\{2.0, 1.2, 0.45\}$. At all levels of noise, the fuzzy activation map obtained by FFM were more superior than SPM. The advantage is more obvious at higher level of noise, demonstrating the robustness of FFM to correlated noise. This results on group study also show that FFM is better at dealing with hemodynamic variability across subjects.

Figure 4 shows three different HRF for generation of synthetic fMR time-series. Our feature extraction procedure is able to capture the variability of HRF and to automatically learn this knowledge by incremental training. This could be proved by the parameters (the center of input features) in the three final fuzzy models, which were built on each time-series, respectively, as indicated in table in Fig. 4. By comparing to HRFs in Fig. 4, we can see that since the delay of response and undershoot for HRF-1 and –3 is smaller than HRF-2, the distance between the input centers of feature F_4 (time ratio at peak amplitude for QHC) and feature F_5 (time ratio at lowest amplitude for QHC) in activated and non-activated class are smaller in fuzzy model of HRF-1 and –3 than in fuzzy model of HRF-2. Moreover, since HRF-2 has little undershoot than the other two HRFs, the distance between input centers of feature F_2 (area difference ratio for QHC) in activated and non-activated class are larger in fuzzy model of HRF-2 than the other two. Thus, the fuzzy feature model is able to capture HRF properties accurately and incremental learning is able to build different fuzzy models to account for HRF variability.

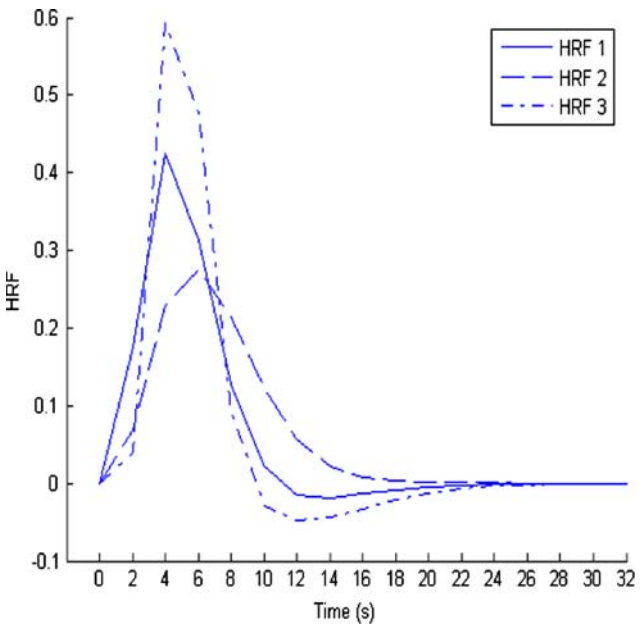

HRF	F_1	F_2	F_3	F_4	F_5
1	0.81 (0.10)	2.86 (0.86)	0.51 (-0.08)	0.49 (0.11)	0.65 (0.02)
2	0.81 (0.14)	3.10 (0.89)	0.50 (-0.02)	0.58 (0.10)	0.80 (0.06)
3	0.82 (0.10)	2.97 (0.86)	0.54 (-0.08)	0.53 (0.09)	0.66 (0.01)

Fig. 4 Correlation between HRF properties and parameters in the developed fuzzy feature models. *Top* three HRFs for synthetic time-series generation; *Bottom* the input centers of five features in the developed fuzzy models. The *numbers* in the outside and inside the brackets are the input center for activated and non-activated class respectively

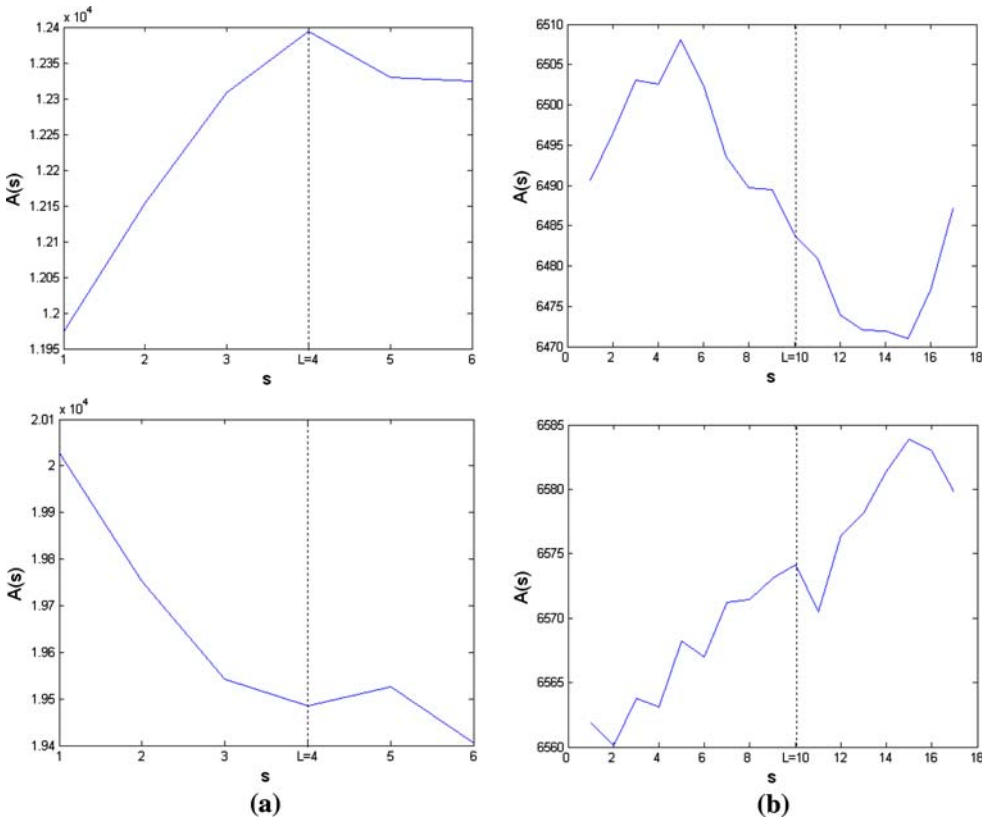

Fig. 5 QHC extracted from fMRI data of visual (**a**) and motor (**b**) task for: activated (*top*) and non-activated (*bottom*) voxels, respectively

3.2 Real data

3.2.1 Visual task

A set of real fMRI data obtained from experiments with a visual task were analyzed, see [18] for further details about this data set. For SPM analysis, all functional images were first corrected for movement artifacts, resampled, and smoothed with a 3D Gaussian filter having FWHM = 4.47 mm. *F*-contrast is used for statistical analysis in SPM2 based on canonical HRF plus time and dispersion derivatives as basis function. Voxels with $p < 0.05$ corrected using family-wise-error (FWE) is determined to be activated. For FFM approach, same parameters were used as for synthetic data.

Note that QHC is also variable across subjects, brain regions and tasks and QHCs in other regions are not of the exact same shape. Nevertheless, their characteristics of QHCs often comprise of similar discriminating features. This is illustrated by Fig. 5 showing typical Quasi-hemodynamic curve (QHC) for activated voxel (top) and non-activated voxel (bottom) in real fMRI data of visual (a) and motor (b) task, respectively. Despite of the difference between QHCs of these two tasks, it is evident that activated and non-activated voxel have quite different QHC shapes in both brain regions and hence common discriminating features could still be discovered with lower degrees of uncertainty. Figure 6 shows the detected activated regions for visual task on a single slice of one subject by both SPM and FFM approach. Since there are no ground truth, it is rather difficult to compare the activation patterns, but still expected activation was found in visual cortex for both approaches.

3.2.2 Group study of silent reading task

Real fMRI data gathered on a silent reading task were used to evaluate the performance of FFM on group study. The

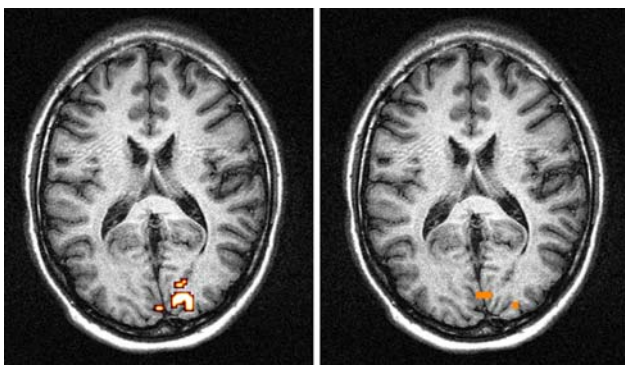

Fig. 6 Detected activation on selected axial slice by SPM (*top*) and FFM (*bottom*) for visual task

dataset consists of six subjects and the task is involved of silent reading of words and pseudowords as soon as they appear on the screen with the resting condition (fixating to a cross in the middle of the screen). The data for each subject contains 360 volume images ($T = 360$) and TR = 2 s; see [10] for more details. The objective is to identify common brain regions for silent reading in all conditions from fMRI time-series of six subjects.

Same parameter settings as in experiments with synthetic data was applied to the group study of this set of real fMRI data except the thresholds ($\zeta_1 = 0.75$, $\zeta_2 = 0.3$). SPM analysis also followed the standard procedure and the group study was performed using a fixed-effect analysis (FFX). Significant hemodynamic changes for reading effects were assessed using the *t*-statistical parametric maps and Family-Wise-Error-Rate (FWER) correction ($p < 0.05$) [23] was performed for multiple comparison in statistical inference. Figure 7 shows significant activated brain regions detected by SPM and FFM. The results are very similar with each other: the activations were found in

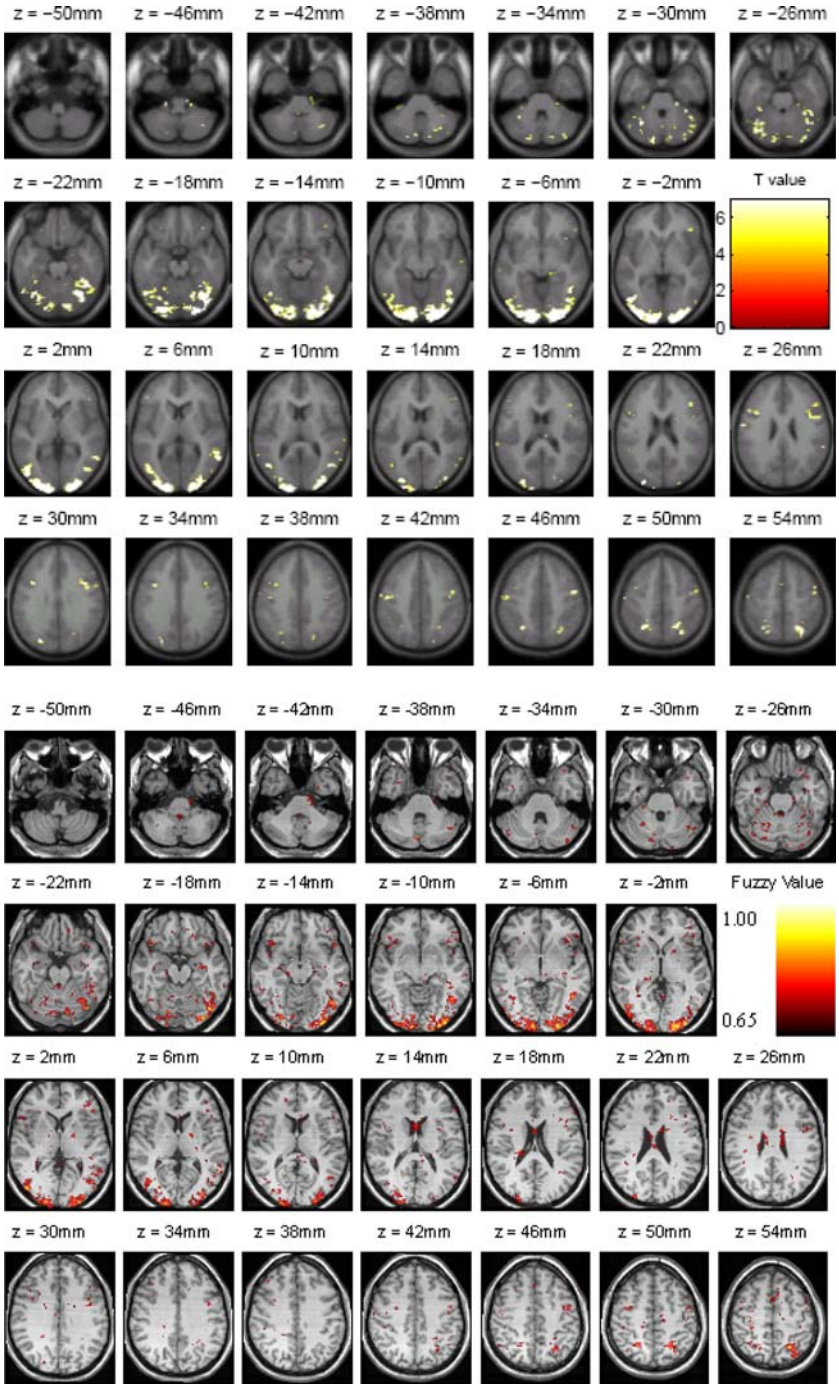

Fig. 7 Detected activation on selected axial slices by SPM (*top*) and FFM (*bottom*) for silent reading task on a group of six subjects

bilateral extrastraite cortices, superior parietal lobes, middle temporal cortices, inferior frontal sulei, middle frontal cortices and cerebellum, which are consistent with previous literature [25].

4 Conclusion

By a novel fuzzy feature extraction method, we are able to convert 4D fMRI datasets into a much simpler and robust feature space to detect functional activation of the brain. A fuzzy feature model (FFM) was first built on a limited prior knowledge represented by a canonical initial training set and thereafter enhanced by incremental learning taking into account the variability of HRF across subjects. A general two-way thresholding scheme was proposed to obtain true activation regions effectively from resulting fuzzy activation maps. Experiments on both synthetic and real fMRI data showed that our FFM approach is less vulnerable to correlated noise and more sensitive to discover weak signals.

Activated and non-activated voxels for the condition of interests are discovered simultaneously and explicitly. Group study on both synthetic and real fMRI data further illustrates that FFM can handle correlated noise and the variability of HRF across subjects. Moreover, the resulting parameters of the fuzzy model could give us meaningful relationships between input features and the type of voxels. As seen in the synthetic group study, the resulting parameters for activated and non-activated voxels in fuzzy features of each subject correlate well with its own HRF properties. Present algorithm can be easily extended to handle and compare multiple conditions through fusion of fuzzy activation maps. Our future work includes taking into account the spatial variability of HRF within a single subject, incorporating variability of brain structures [27] and tissue classes [17] across subjects, and applying to multi-modality imaging techniques [16].

References

1. Andersen AH, Gash DM, Avison MJ (1999) Principal component analysis of the dynamic response measured by fMRI. Magn Reson Imaging 17(6):795–815
2. Benjamini Y, Hochberg Y (1995) Controlling the false discovery rate: a practical and powerful approach to multiple testing. J R Stat Soc Ser B 57:289–300
3. Bullmore E, Long C, Fadili J, Calvert G, Zalaya F, Carpenter TA, Brammer M (2001) Colored noise and computational inference in neuophysiological (fMRI) time series analysis: resampling methods in time and wavelet domains. Hum Brain Mapp 12:61–78
4. Biswal B, Ulmer J (1999) Blind source separation of multiple signal sources of fMRI data sets using independent component analysis. J Comput Assist Tomogr 23(2):265–271
5. Chuang K, Chiu M, Lin C, Chen J (1999) Model-free functional MRI analysis using Kohonen clustering neural network and fuzzy c-means. IEEE Trans Med Imaging 18:1117–1128
6. Friston KJ, Holmes AP, Worsley KJ, Poline J-B, Frith CD, Frackowiak RSJ (1995) Statistical parametric maps in functional imaging: a general linear approach. Hum Brain Mapp 2:189–210
7. Hossein-Zadeh GA, Soltanian-Zadeh H, Ardekani BA (2003) Multiresolution fMRI activation detection using translation invariant wavelet transform and statistical analysis based on resampling. IEEE Trans Med Imaging 22(3):302–314
8. Lu W, Rajapakse JC (2005) Approach and applications of constrained ICA. IEEE Trans Neural Netw 16(1):203–212
9. Lu W, Rajapakse JC (2006) ICA with reference. Neurocomputing 69:2244–2257
10. Mechelli A, Friston KJ, Price CJ (2000) The effects of presentation rate during word and pseudoword read: a Comparison of PET and fMRI. Cogn Neurosci 12:145–156
11. McKeown MJ, Makeig S, Brown GG, Jung TP, Kindermann SS, Bell AJ, Sejnowski TJ (1998) Analysis of fMRI data by blind separation into independent spatial components. Hum Brain Mapp 6:160–188
12. Meyer-Baese A, Wismueller A, Lange O (2004) Comparison of two exploratory data analysis methods for fMRI: unsupervised clustering versus independent component analysis. IEEE trans Info Technol Biomed pp 387–398
13. Ngan S, Hu X (1999) Analysis of functional magnetic resonance imaging data using self-organizing mapping with spatial connectivity. Mgn Reson Med 41:939–946
14. Ogawa S, Tank D, Menon R (1992) Intrinsic signal changes accompanying sensory simulation: Functional brain mapping with magnetic resonance imaging. Proc Natl Acad Sci 89:5951–5955
15. Ross TJ (2004) Fuzzy logic with engineering applications, 2nd edn. Wiley, London, pp 213–241
16. Rajapakse JC, DeCarli C, Mclaughlin A, Giedd JN, Krain AL, Hamburger SD, Rapoport JL (1996) Cerebral magnetic resonance image segmentation using data fusion. J Comput Assist Tomogr 20(2):206–218
17. Rajapakse JC, Giedd JN, DeCarli C, Snell JW, McLaughlin A, Vauss YC, Krain AL, Hamburger S, Rapoport JL (1996) A technique for single-channel MR brain tissue segmentation: application to a pediatric sample. Magn Reson Imaging 14(9):1053–1065
18. Rajapakse JC, Kruggel F, Maisog JM, von Cramon DY (1998) Modeling hemodynamic response for analysis of functional MRI time-series. Hum Brain Mapp 6:283–300
19. Rajapakse JC, Piyaratna J (2001) Bayesian approach to segmentation of statistical parametric maps. IEEE Trans Biomed Eng 48:1186–1194
20. Welcome Department of Imaging Neuroscience, Statistical Parametric Mapping, http://www.fil.ion.ucl.ac.uk/spm/, 2004
21. Vazquez AL, Noll DC (1998) Nonlinear aspects of the bold response in functional mri. Hum Brain Mapp 40:249–260
22. Woolrich MW, Jenkinson M, Brady JM, Smith SM (2004) Fully Bayesian spatio-temporal modeling of fMRI data. IEEE Trans Med Imaging 24(2):213–231
23. Worsley KJ, S.Marrett, Neelin P, Vandal AC, Friston KJ, Evans AC (1996) A united statistical approach for determining significant signals in images of cerebral activation. Hum Brain Mapp 4:58–73
24. Wang Y, Rajapakse JC (2006) Contextual modeling of functional MR images with conditional random fields. IEEE Trans Med Imaging 25(6):804–812
25. Zheng X, Rajapakse JC (2006) Learning functional structure from fMR images. Neuroimage 31(4):1601–1613
26. Zhou J, Rajapakse JC (2006) Extraction of fuzzy features for detecting brain activation from functional MR time-series, neural information processing. Lecture Notes on Computer Science 4243:983–992
27. Zhou J, Rajapakse JC (2005) Segmentation of subcortical brain structures using fuzzy templates. Neuroimage 28(4):927–936